Available online at www.sciencedirect.com
ScienceDirect
Journal of the European Ceramic Society 29 (2009) 505–516
www.elsevier.com/locate/jeurceramsoc

Correlation between phase evolution, mechanical properties and instrumented indentation response of TiB_2-based ceramics

Amartya Mukhopadhyay [a,*], G.B. Raju [a], Bikramjit Basu [a], A.K. Suri [b]

[a] *Laboratory for Advanced Ceramics, Department of Materials and Metallurgical Engineering, Indian Institute of Technology, Kanpur, India*
[b] *Materials Group, Bhabha Atomic Research Center, Mumbai, India*

Received 15 April 2008; received in revised form 24 June 2008; accepted 24 June 2008
Available online 9 August 2008

Abstract

In densifying non-oxide high temperature ceramics, like titanium di-boride (TiB_2), the type and amount of sinter-aid critically determine the microstructural developments and consequently the mechanical properties. In this perspective, the present work is carried out to assess the feasibility whether $MoSi_2$ addition (up to 10 wt.%) can potentially improve the mechanical properties (hardness, fracture toughness, flexural strength), while enhancing the densification behaviour of TiB_2. In order to answer such an important issue and to understand the mechanisms contributing to the variations in mechanical properties, we have evaluated sharp instrumented indentation response (2 N load) of a range of hot pressed TiB_2–$MoSi_2$ compositions. In addition, the Vickers indentation data obtained at macro load (up to 100 N) are also analyzed. Our experimental results reveal that the addition of only 2.5 wt.% $MoSi_2$ to TiB_2 results in the attainment of high sinter density (>99% ρ_{th}), after hot pressing at 1700 °C. The dense TiB_2–2.5 wt.% $MoSi_2$ composite composition has been found to possess a good combination of mechanical properties, including high hardness (H_{v5}∼30 GPa) and moderate fracture toughness (∼6 MPa $m^{1/2}$). Furthermore, the four-point flexural strength values vary in the range of 370–400 MPa, with the maximum value for 2.5 wt.% $MoSi_2$ containing composite. Interestingly, an increase in the additive ($MoSi_2$) content above 5 wt.% degrades the mechanical properties. The degradation in mechanical properties has been attributed to the presence of secondary phases (Ti_5Si_3, Mo_5Si_3) and its effect has been critically analyzed. The mechanical response data, recorded using depth sensing instrumented Vickers indenter has been analyzed in the light of the elastic/plastic work done, and the elastic modulus (E) values, as computed from the initial slopes of unloading curves, have been found to vary in the range of 460–500 GPa. Additionally, the analysis of macro Vickers hardness measurements reveal 'indentation-size effect', which has been discussed in terms of mechanical response at the indented zone, and in correlation with the material properties.

Keywords: TiB_2; $MoSi_2$; Hot pressing; Phase evolution; Mechanical properties

1. Introduction

TiB_2 is a material of growing interest amongst the various ultra-high temperature ceramics (UHTC), due to its characteristic high melting point (∼3200 °C), high hardness and strength retention at elevated temperatures, good thermal and electrical conductivities and high wear resistance.[1–4] This unique combination of properties renders TiB_2-based materials suitable for a wide range of technological applications, such as armor materials, wear components, conductive coatings, cathode materials for Hall-Heroult cell, aluminum evaporation boats and electro discharge machining (EDM) electrodes.

However, consolidation difficulties and poor fracture toughness (∼4 MPa $m^{1/2}$) generally restrict their widespread applications. The densification of monolithic TiB_2 requires extremely high sintering temperatures of up to ∼2100 °C and long holding times due to the predominant covalent bonding and the low self diffusion coefficient.[2,5–9] Such extreme processing conditions result in exaggerated grain growth of the as-sintered materials, leading to degradation of mechanical properties.[9,10] Till date, most research efforts, concerned with sintering of TiB_2-based materials at relatively lower temperatures, have explored the use of various metallic binders (Fe, Ni, Cr, Co).[2,5,7,8,11–13] Though such experiments have demonstrated

* Corresponding author. Tel.: +91 512 2597771; fax: +91 512 2597505.
E-mail address: amartya.28nov@gmail.com (A. Mukhopadhyay).

0955-2219/$ – see front matter © 2008 Elsevier Ltd. All rights reserved.
doi:10.1016/j.jeurceramsoc.2008.06.030

the possibility of obtaining dense TiB_2-based cermets at lower temperatures, the presence of metallic sinter-additives result in significant degradation of the high temperature properties and corrosion resistance of TiB_2.

To overcome such limitations, in recent times, efforts have been directed towards exploring the possibilities of obtaining dense TiB_2-based ceramics, with better mechanical properties, by replacing metallic binders with ceramic sinter-additives.[2,14–19] It has been observed that while use of metallic phases in very limited amounts (<2 wt.%) permits near theoretical densification of TiB_2, comparatively higher amounts (>5 wt.%) of ceramic additives are required to obtain similar sinter densities.[2] Furthermore, the published results reveal that incorporation of ceramic sinter-additives, above a critical fraction, often results in deterioration of the mechanical properties.[2,14,15] In this backdrop, although there are limited reports concerning the mechanical properties possessed by TiB_2-based materials containing different ceramic sinter-additives,[2,14–19] critical analysis of the correlation between the amounts of ceramic additives present and their effects on the microstructural development and concomitantly the various mechanical properties of TiB_2 is currently lacking.

Following our previous results of TiB_2–(10–20) wt.% $MoSi_2$[9] and in the light of literature results implying deterioration of mechanical properties at higher additive contents,[2,14,15] in the present work we have attempted to explore the possibility of developing dense (>99% ρ_{th}) TiB_2-based ceramics, with improved mechanical properties, using lesser amount of $MoSi_2$ (up to 10 wt.%). The mechanical properties of the developed TiB_2-based materials, reinforced with different amounts of $MoSi_2$ additive (0–10 wt.%), have been investigated in detail. It must be pointed out here that $MoSi_2$ has been selected as sinter-additive, due to its good combination of properties like, high melting point (~2020 °C), good oxidation resistance (up to 1700 °C) and good thermal and electrical conductivities.[20] Based on the analysis of the correlation between phase evolution and mechanical behaviour results, we have made an attempt to critically explore the effects of $MoSi_2$ content on the resultant mechanical properties, which allow us to optimize the sintering parameters and composition to develop TiB_2-based ceramics with superior performance.

2. Experimental details

2.1. Starting powders

The starting powders used in the present work are in-house processed TiB_2 and $MoSi_2$. TiB_2 powders were synthesized via boron carbide reduction reaction of commercial TiO_2 powders (>99% purity, Merck, Germany), B_4C (in-house synthesized) and high purity (>99% purity) petroleum coke (M/s Assam carbon, Guwahati, India). $MoSi_2$ was synthesized from elemental powders Mo (>99% purity, supplier Leco Industries, USA) and Si (>99% purity, supplier Merck, Germany). More details of preparation of the starting powders are reported elsewhere.[9]

The presence of oxygen (~0.5 wt.%), carbon (~0.6 wt.%) and nitrogen (~0.6 wt.%), as the major impurities in the as synthesized TiB_2, were determined by vacuum fusion analysis technique (Leco Industries, USA). The mean particle diameters and specific surface areas of the starting powders were evaluated using the laser particle analyzer (analysett 22) and BET (COULTER, SA300), respectively. The TiB_2 powders possessed an average particle size (D_{50}) of 2 μm and specific surface area 1.491 m^2/g, while the coarser $MoSi_2$ powders were characterized by D_{50} of 3.4 μm and specific surface area of 0.289 m^2/g.

2.2. Processing

TiB_2 and $MoSi_2$ powders were ground and mixed, using WC grinder, in proportions corresponding to various compositions (TiB_2–x wt.% $MoSi_2$; $x = 0$, 2.5, 5, 7.5 and 10). The sintering of the monolithic TiB_2, and TiB_2 ceramics containing various proportions of $MoSi_2$ sinter-additive, were performed via hot pressing (HP). The hot pressing experiments were carried out using 12.2 mm diameter graphite die, in vacuum (10^{-5} Pa) with a maximum applied pressure of 30 MPa at the holding temperature. Holding temperature was varied between 1600 and 1800 °C (heating rate: 15 °C/min), with a holding time of 1 h. After the completion of sintering, vacuum and pressure were maintained till the end of cooling. The thickness of the hot pressed pellets were ~7–9 mm. Additionally, in order to make flexural strength test samples, hot pressed disks of 65 mm diameter and 5 mm thickness were fabricated. For further characterizations, specimens of required dimensions were machined using wire cut electric discharge machining (EDM). In the following, the ceramic composites hot pressed from starting powders containing TiB_2–x wt.% $MoSi_2$ are referred to as *TxM*.

2.3. Characterization

The densities of samples were measured in water according to Archimedes' principle. For estimating the % densification (%ρ_{th}), the measured densities were compared with the theoretical densities, estimated using rule of mixture for the composites. The phase identification was performed by X-ray diffraction (XRD) using Cu Kα radiation (Rigaku, Japan). Microstructural observations of the polished as well as fractured surfaces were performed using scanning electron microscopy (FE-SEM, JSM-6330F). For revealing the TiB_2 grains, polished surfaces of some of the samples were chemical etched using 10 HCl–1 HNO_3 aqueous solution at room temperature for 15 s. Detailed compositional analysis of the various observed phases was performed using Energy Dispersive Spectrometer (EDAX, JSM-6330F), attached with SEM.

In order to measure the hardness and toughness, smoothly polished surfaces were subjected to Vickers Indentation, with indent load varying between 2 and 100 N (dwell time: 15 s), using a Universal Hardness tester. For further understanding of the mechanical behaviour, depth sensing instrumented indentations was performed, at a peak load of 2 N, using an instrumented Vickers indenter (CSM international, MTT SN: 02-0113). The load vs. penetration depth curves was obtained at a loading and unloading rate of 0.017 N/s, with a holding time of 15 s at the peak load. The fracture toughness was evaluated by crack length

Table 1
Sinter densities (as % densification), microstructural phase assemblage and mechanical properties of the hot pressed monolithic TiB_2 and the various $MoSi_2$ containing TiB_2-based composites

Material	Hot pressing temperature (°C)	% Densification (% ρ_{th})	Crystalline phases detected by XRD	Hardness (at load = 0.2 kg) $H_{v0.2}$ (GPa)	Hardness (at load = 5 kg) H_{v5} (GPa)	Hardness (at load = 10 kg) H_{v10} (GPa)	Fracture toughness (at load = 5 kg) K_{IC} (MPa m$^{1/2}$)	Four-point flexural strength (MPa)
Monolithic TiB_2	1700	90.5	TiB_2	20.8 ± 0.8	19.7 ± 1.5	20.3 ± 1.0	4.08 ± 0.21	–
Monolithic TiB_2	1800	96.1	TiB_2	32.44 ± 0.45	28.6 ± 0.53	24.0 ± 1.4	4.64 ± 0.45	367.1 ± 52.5
T2.5M	1700	99.1	TiB_2, $MoSi_2$, Mo_5Si_3, Ti_5Si_3	32.89 ± 0.16	29.95 ± 0.31	26.9 ± 1.9	5.69 ± 0.35	390.5 ± 31.1
T5M	1700	98.8	TiB_2, $MoSi_2$, Mo_5Si_3, Ti_5Si_3	32.63 ± 0.25	29.9 ± 0.17	26.2 ± 1.1	5.04 ± 0.32	389.1 ± 26.1
T7.5M	1700	97.4	TiB_2, $MoSi_2$, Mo_5Si_3, Ti_5Si_3	30.55 ± 0.24	25.64 ± 0.79	24.9 ± 1.4	4.2 ± 0.74	–
T10M	1700	96.7	TiB_2, $MoSi_2$, Mo_5Si_3, Ti_5Si_3	24.61 ± 0.49	22.97 ± 0.44	22.3 ± 1.4	4.66 ± 0.46	267.8 ± 69.6

measurement of the radial crack pattern formed around Vickers indents, adopting formulation proposed for radial-median crack systems, by Anstis et al.[21] It is to be noted here that, since the c/a (where c = half crack length of a radial crack and a = half diagonal length of an indent) ratios, calculated from the SEM images of the indentation induced cracking, are ≥3, the developed crack system can be classified as radial-median (half-penny cracks).[21–25] The reported values are the average of data obtained from at least five indentation tests. Furthermore, the indentation damage behaviour of materials was studied in details using SEM. For flexural strength measurements, specimens were machined into bar shapes with dimensions of 3 mm × 4 mm × 40 mm. The edges of all the specimens were chamfered, to minimize the effect of stress concentration due to machining flaws. The flexural strengths were measured in a four-point bending configuration, at a crosshead speed of 0.5 mm/min and inner and outer spans of 10 and 30 mm, respectively, using a universal testing machine (INSTRON 4465, USA). The reported flexural strength values are an average of at least five samples.

3. Results

3.1. Densification, phase evolution and microstructure

The sinter densities (as % densification; % ρ_{th}) of the hot pressed samples are presented in Table 1. It can be observed that monolithic TiB_2 could be densified to only ∼91% of the theoretical density on hot pressing at 1700 °C. However, raising the temperature to 1800 °C results in achieving ∼96% ρ_{th} with monolithic TiB_2 (HP; 1800 °C), which is in accordance with earlier reports.[9,26,27] Further observation of Table 1 reveals that the addition of only a small amount (2.5 wt.%) of $MoSi_2$ to TiB_2 (T2.5M) leads to the achievement of ∼99% ρ_{th}, even on hot pressing at the lower temperature of 1700 °C. Hence $MoSi_2$, as sinter-additive, is effective in obtaining near theoretical densification of TiB_2-based ceramics at lower processing temperature. However, with the increase in $MoSi_2$ additive content (up to 10 wt.%), the sinter densities (HP; 1700 °C) appear to decrease to a modest extent, although the densities of all the $MoSi_2$ containing composites are still higher than that of monolithic TiB_2 (HP; 1800 °C).

XRD patterns, recorded with the hot pressed samples are presented in Fig. 1a. The characteristic peaks, corresponding to only TiB_2, can be observed in the pattern obtained with hot pressed monolithic TiB_2. However, XRD investigation of the hot pressed $MoSi_2$ containing TiB_2 ceramics (HP; 1700 °C) reveals the presence of Ti_5Si_3 and Mo_5Si_3, in addition to major phases (TiB_2 and $MoSi_2$). The various secondary phases present in the TiB_2-based composites are reported in Table 1. From the relative intensities of the XRD peaks, it can be qualitatively envisaged that the amounts of the secondary phases present (in particular, Mo_5Si_3 and Ti_5Si_3) after hot pressing considerably increase with the initial $MoSi_2$ content of the starting powders (see Fig. 1a). Since no such secondary phases could be detected either in the starting powders (not shown) or in hot pressed monolithic TiB_2, it can be realized that such phase formation is mainly due to sintering reaction between TiB_2 and $MoSi_2$. The discussion on

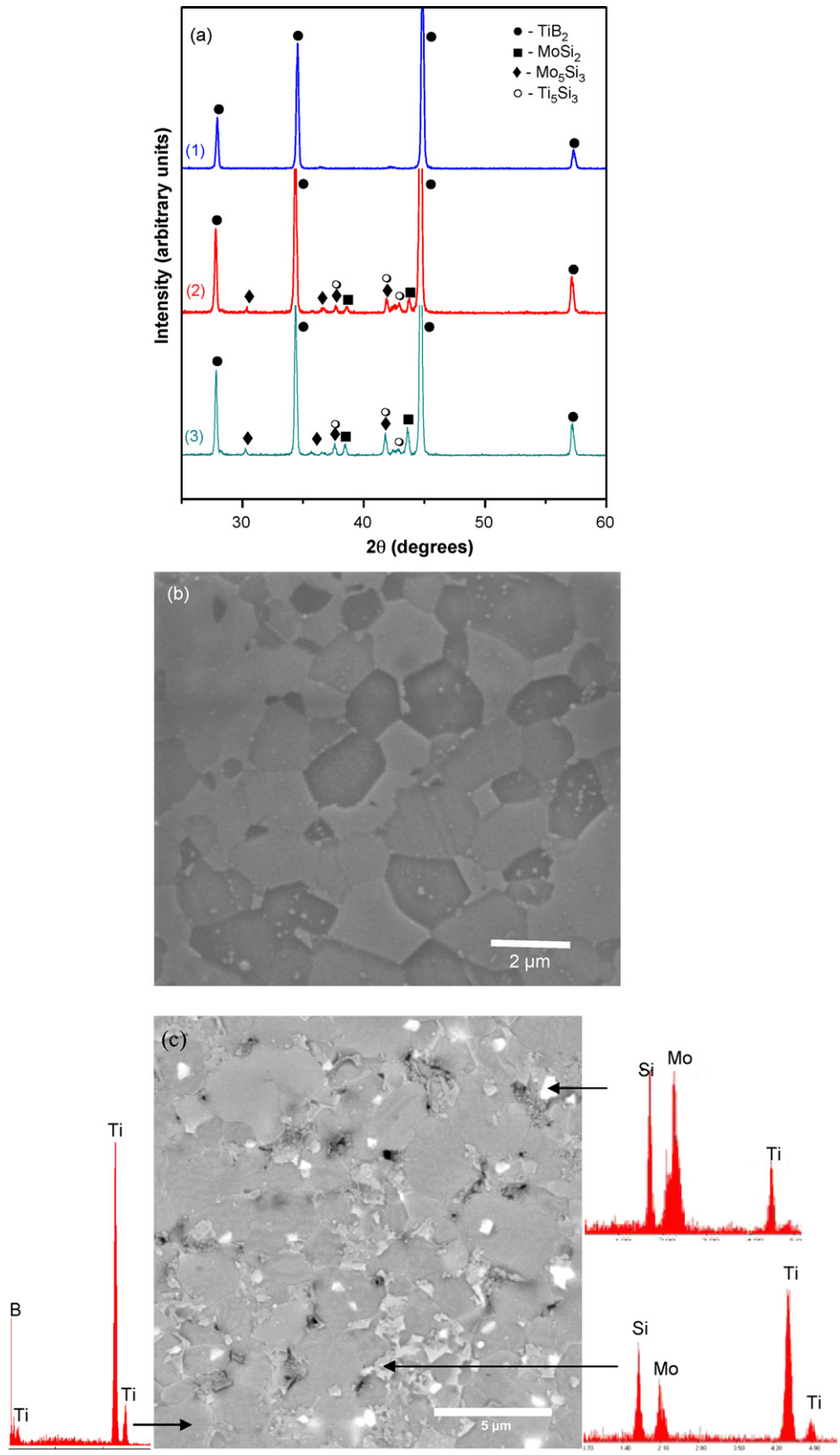

Fig. 1. (a) XRD patterns recorded with hot pressed monolithic TiB_2 (1), T5M (2) and T10M (3), showing the presence of various reaction product phases in the $MoSi_2$ reinforced TiB_2-ceramics; (b) secondary electron mode SEM micrograph of polished-etched surface of monolithic TiB_2 (HP; 1800 °C) showing the presence of equiaxed grains of nearly similar sizes; and (c) back scattered SEM micrograph obtained from the polished surface of T5M, hot pressed at 1700 °C. EDS patterns recorded from the different microstructural phases are also shown.

possible sintering reactions is beyond the scope of the present paper.

Fig. 1b presents a representative SEM micrograph of polished and etched surface of hot pressed monolithic TiB_2 (HP; 1800 °C). From the SEM micrograph, no evidence of any secondary phase can be found. Careful observation of the grain morphology reveals that the grains are fairly equiaxed in shape with the grain sizes varying between 2 and 3 μm. Typical back scattered SEM (BSE) micrograph, along with EDS patterns collected from specific microstructural regions present on the polished and chemically etched surfaces of the $MoSi_2$ containing TiB_2 (T5M), is shown in Fig. 1c. The BSE contrast, along with the etching induced topography, reveals the presence of three distinct phases. In correlation with the XRD results (Fig. 1a), the EDS patterns obtained from the respective phases indicate that the grey phase, constituting the major area fraction of the micrographs, corresponds to TiB_2, while the phase appearing brightest in contrast and located in the intercrystalline regions as well as within the matrix (TiB_2) grains corresponds to $MoSi_2$. A fraction of the bright regions might also correspond to the reaction product phase, Mo_5Si_3. One of the most notable observations is the presence of a still different phase along the grain boundaries and triple points of the matrix TiB_2 grains. EDS patterns obtained from such intergranular phase shows the presence of stronger Ti and Si peaks (Fig. 1c). Such microstructural and EDS observations, in cognizance with the XRD results (Fig. 1a), reveal that the phase corresponds to the reaction product phase, Ti_5Si_3, which is located mostly along the intercrystalline regions of the TiB_2 grains. The matrix grain sizes of these TiB_2-based composites are found to vary between 2 and 4 μm.

Observation of the fractured surface of monolithic TiB_2 (HP; 1800 °C), as obtained from room temperature flexural strength tests, reveals a predominantly intergranular mode of fracture, with very minimal contribution from transgranular fracture mode (Fig. 2a). However, the fracture mode changes considerably with increase in the additive content. The fractured surfaces of the composites reveal a predominant contribution from transgranular fracture (Fig. 2b and c). Furthermore, on critical observation it becomes obvious that, as compared to the fractured surface of T5M (Fig. 2b), the fractured surface of T10M (Fig. 2c) reveals some additional contribution from the intergranular fracture mode. The reasons are discussed in Section 4.

3.2. Hardness properties

The mechanical properties of the various hot pressed TiB_2-based ceramics/composites, developed in the present work, are reported in Table 1. It can be observed that, regardless of the indent load (2, 50 or 100 N), the hardness of the TiB_2-based materials follow a nearly constant trend in variation with $MoSi_2$ additive content and sinter density. In correlation with the densification result, an increase in hot pressing temperature from 1700 to 1800 °C leads to improvement of hardness (H_{v5}) of monolithic TiB_2 from ~20 GPa (91% ρ_{th}) to ~29 GPa (96% ρ_{th}). Furthermore, with addition of only small

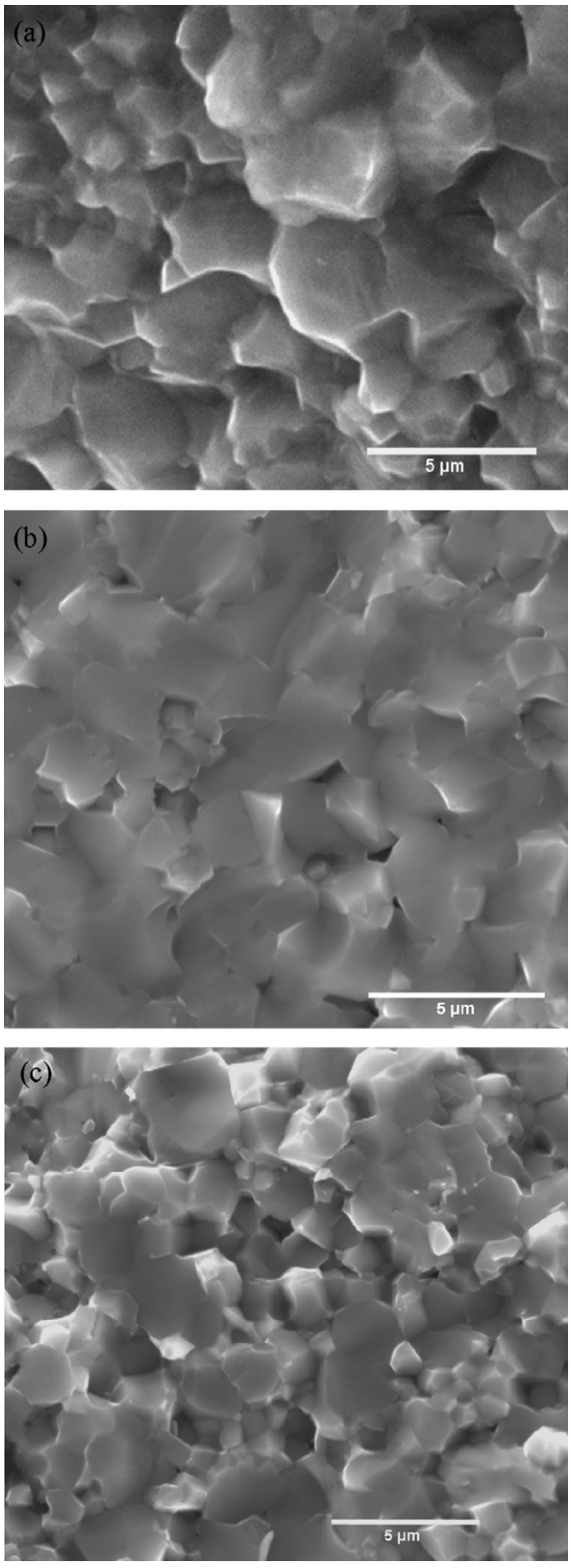

Fig. 2. Secondary electron SEM images of fractured surfaces obtained during room temperature flexural tests of (a) monolithic TiB_2 (HP; 1800 °C); (b) T5M and (c) T10M (HP; 1700 °C). Note the effect of secondary phases content on the fracture mode.

amount (2.5 and 5 wt.%) of $MoSi_2$ (sinter-additive), modest improvement in hardness (H_{v5}~30 GPa) can be noticed for the composites, sintered at the optimized hot pressing temperature of 1700 °C. It is pertinent to note that, even though $MoSi_2$ is softer (H_v~13 GPa)[28] than TiB_2, addition of small amount of $MoSi_2$ to TiB_2 does not have detrimental effect on the hardness. This can be attributed to the considerable improvement in sinter density (~99% ρ_{th}) on reinforcement with 2.5–5 wt.% $MoSi_2$. However, it is observed that hardness decreases significantly with further increase in $MoSi_2$ additive content. The synergistic effect of decrease in sinter density, along with the presence of higher volume fraction of softer $MoSi_2$ and other reaction product phases, is responsible for this abasement of hardness at $MoSi_2$ (sinter-additive) content >5 wt.%. A comparison of the hardness possessed by TiB_2-based ceramics, using $MoSi_2$ as sinter-additive, with those achieved on using other ceramic sinter-additives is presented in Fig. 3. The variation of hardness with amount of other ceramic sinter-additives correlates well with the current observation. More importantly the use of $MoSi_2$ as additive, in comparison to other ceramic sinter-additives, results in higher hardness of TiB_2-based ceramics. Consideration should also be given to the fact that the relatively finer grain sizes (~3 μm) of the present materials also contributes to higher hardness.

An interesting observation has been the considerable reduction in hardness of the hot pressed TiB_2-based ceramics/composites, as measured with Vickers indents obtained with increase in indent load (2–100 N). A plot showing the variation in measured hardness with indent load is presented in Fig. 4. It can be noted that monolithic TiB_2 (HP; 1800 °C) and $MoSi_2$ reinforced TiB_2-based composites (HP; 1700 °C) exhibit comparatively higher hardness as measured with Vickers indents obtained at the lower indent loads than those obtained at higher loads. However, monolithic TiB_2, hot pressed at 1700 °C, exhibit very low hardness at all indent loads, which does not vary with load to any noticeable extent. Such interesting observations will be more critically analyzed in Section 4.

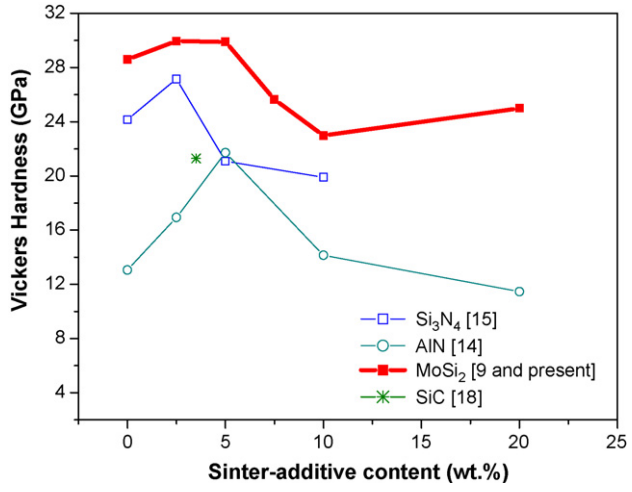

Fig. 3. Variation of Vickers hardness of TiB_2-based ceramics reinforced with varying amount of different ceramic sinter-additives.

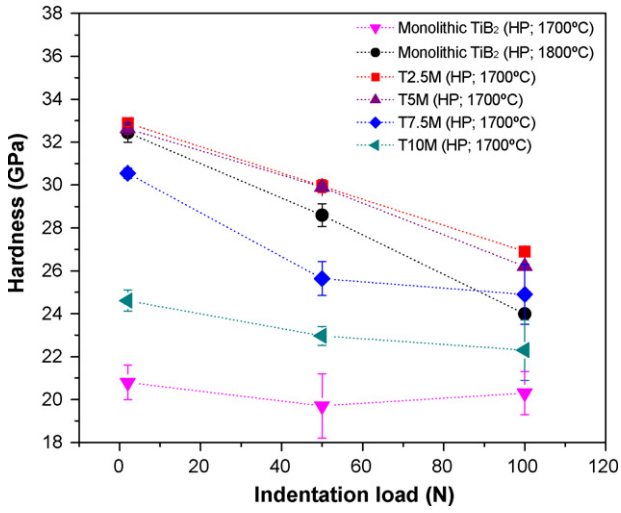

Fig. 4. Variation of Vickers hardness with indent load for monolithic TiB_2 (HP; 1800 °C) as well as monolithic TiB_2 and TiB_2-based ceramics, reinforced with the various amounts of $MoSi_2$ (HP; 1700 °C).

3.3. Depth sensing instrumented indentation response

Some useful mechanical property data, along with critical analysis of indentation response, have been extracted from load vs. penetration depth measurements, performed at a peak load of 2 N, using instrumented Vickers indenter (see Fig. 5a). It can be observed that the variation of residual indentation depths, after completion of the unloading cycle, correlates well with the measured hardness variation with $MoSi_2$ content. Here it must be recalled that hardness is an indication of the amount of plastic deformation occurring in a given material at a particular indent load. Hence, using the load vs. penetration curves (*P–d* curves), an exploratory attempt has been made to investigate the correlation between the experimentally determined Vickers hardness values ($H_{v0.2}$; measurement of indent diagonal lengths), with the estimated plastic work done under the indent load, for all the densified materials. Following the methodology used by Chollacoop and co-workers,[29] area under the loading curve is considered to be the total work done during indentation (W_t), with the area under the unloading curve being the recovered elastic work (W_e). The net plastic work performed during indentation, at the specified load (W_p), can be obtained as

$$W_p = W_t - W_e \quad (1)$$

The characteristic areas corresponding to W_e and W_p are indicated in a typical *P–d* curve shown in Fig. 5b and the corresponding values, for the investigated TiB_2-based ceramics, are reported in Table 2. A plot representing the variation of the W_p, W_e and $H_{v0.2}$, with wt.% $MoSi_2$ sinter-additive content is shown in Fig. 5c. It can be clearly noticed that reduction in hardness, with increase in $MoSi_2$ content, correlates well with the increase in residual plastic work performed during indentation. Further discussion, relating material properties with the various works done during indentation will be presented in Section 4.

The elastic moduli (E) values, derived from the estimated system modulus by measurement of slopes of the initial part

Table 2
The various works done (W_t, W_e and W_p) and elastic modulus (E), of the densified TiB_2-based ceramics, as determined from instrumented indentation experiments, performed at a peak load of 2 N

Composition	Hot pressing temperature (°C)	Residual plastic work (W_p) ($\times 10^{-6}$ J)	Recovered elastic work (W_e) ($\times 10^{-6}$ J)	Total work done (W_t) ($\times 10^{-6}$ J)	Elastic modulus (E) (GPa)
Monolithic TiB_2	1800	0.701 ± 0.035	0.668 ± 0.037	1.369 ± 0.039	497 ± 15
T2.5M	1700	0.664 ± 0.014	0.721 ± 0.021	1.385 ± 0.022	486 ± 11
T5M	1700	0.688 ± 0.017	0.727 ± 0.019	1.415 ± 0.025	479 ± 12
T7.5M	1700	0.789 ± 0.021	0.728 ± 0.023	1.516 ± 0.028	464 ± 17
T10M	1700	0.894 ± 0.027	0.731 ± 0.025	1.625 ± 0.031	459 ± 16

of the unloading curves, are reported in Table 2. We have followed the methodology proposed by Oliver and Pharr.[30,31] The calculations of E were performed by assuming a Poisson's ratio of 0.2 for the TiB_2-based ceramics. The detailed procedures for estimating elastic modulus from *P–d* curves are mentioned elsewhere.[30–34] It must be noted that the elastic modulus value of ~500 GPa, as estimated from the unloading part of the *P–d* curve for monolithic TiB_2 (HP; 1800 °C), agrees well with the values previously reported using more conventional techniques.[2,18,27] Furthermore, *E*-modulus considerably decreases with the addition of $MoSi_2$ sinter-additive, which can be expected in light of the lower stiffness of $MoSi_2$ and the other secondary phases, as compared to TiB_2.[2]

3.4. Fracture toughness and flexural strength

Fracture toughness, as obtained via short crack method,[25] along with the flexural strengths (four-point bending), of the TiB_2-based ceramics are presented in Table 1. In general, the investigated materials exhibit modest toughness varying between 4 and 6 MPa $m^{1/2}$. An important result is the possibility of slight increment in fracture toughness (up to ~6 MPa $m^{1/2}$) of the nominally brittle TiB_2 ceramics, with small amount of $MoSi_2$ addition (2.5 wt.%). However, the fracture toughness decreases with further increase in $MoSi_2$ content. From the plot (Fig. 6), comparing these fracture toughness values with those previously achieved by using other ceramic additives,[14–18] it can be further observed that toughness increment can be achieved at some optimum reinforcement content, beyond which toughness generally deteriorates, irrespective of the sinter-additive. Regarding flexural strength, Table 1 reveals that it nearly follows nearly similar trend, as fracture toughness, in variation with $MoSi_2$ sinter-additive content. It must be noted that the optimized composition, T2.5M, possess a flexural strength (~400 MPa), which is comparable with most high performance structural ceramic materials.[28] The reasons behind such effects of the amounts of $MoSi_2$ sinter additive on the fracture behaviour of the TiB_2-based composites are discussed in Section 4.

4. Discussion

4.1. Fracture properties

It has been observed that presence of the secondary phases influences the crack propagation path. Such evidences can be found from the fractured surfaces shown in Fig. 2, and the BSE micrograph, corresponding to a polished surface of T10M, as shown in Fig. 7. From the fractured surfaces (Fig. 2), it is evident that on reinforcement with $MoSi_2$, the fracture mode changes from a primarily intergranular to a predominantly transgranular mode. It must be noted here that coefficient of thermal expansions (α) of $MoSi_2$ (~8×10^{-6} K^{-1})[28] and Mo_5Si_3 (5×10^{-6} K^{-1}),[35] are lower than the α, corresponding to the '*c*'-axis, of the hexagonal TiB_2 (~10×10^{-6} K^{-1}).[5] Due to such mismatch in α, modest tensile residual stresses will be generated within some of the TiB_2 grains and compressive residual stresses within $MoSi_2$ or Mo_5Si_3, during cooling from the hot pressing temperature. The presence of tensile radial stresses within the TiB_2 matrix grains weakens the grain interiors, while the grain boundaries are concomitantly strengthened due to action of net compressive residual stresses from either side. As a result, the crack is impeded from propagating along the grain boundaries (otherwise easier propagation path) and deflected towards the grain interiors. Such effects, caused by the presence of $MoSi_2$ and Mo_5Si_3, increase the propensity for transgranular fracture with respect to intergranular fracture. Since fracture energy for cleavage (transgranular) fracture is comparatively higher than that for grain boundary (intergranular) fracture, this change in fracture mode results in modest increase in fracture toughness. More evidences of change in fracture mode to transgranular (indicated by arrows), in the presence of $MoSi_2$ and Mo_5Si_3 (phases with brighter contrast), can also be found on observation of the Vickers indentation (at 100 N) induced crack paths, as shown in Fig. 7. Another mechanism, responsible for the possible toughness increment is crack bridging by the secondary phases. Evidence of considerable impedance to crack propagation, and even complete arrest of a propagating crack, on interaction with $MoSi_2$ and Mo_5Si_3 can be easily observed (indicated by dots) from Fig. 7.

However, for higher $MoSi_2$ containing composites, presence of slightly higher fraction of porosities and brittle reaction products lead to somewhat reduction in interfacial strength of some of the grain boundaries (also see Section 4.2). As a result, some additional contribution of intergranular fracture, at higher $MoSi_2$ content (Figs. 2c and 7), may mask the effects of the mechanisms causing resistance to crack propagation. Hence, fracture toughness improvement is not noticeable in TiB_2-based composites, reinforced with higher amount of $MoSi_2$ sinter-additive (>5 wt.%).

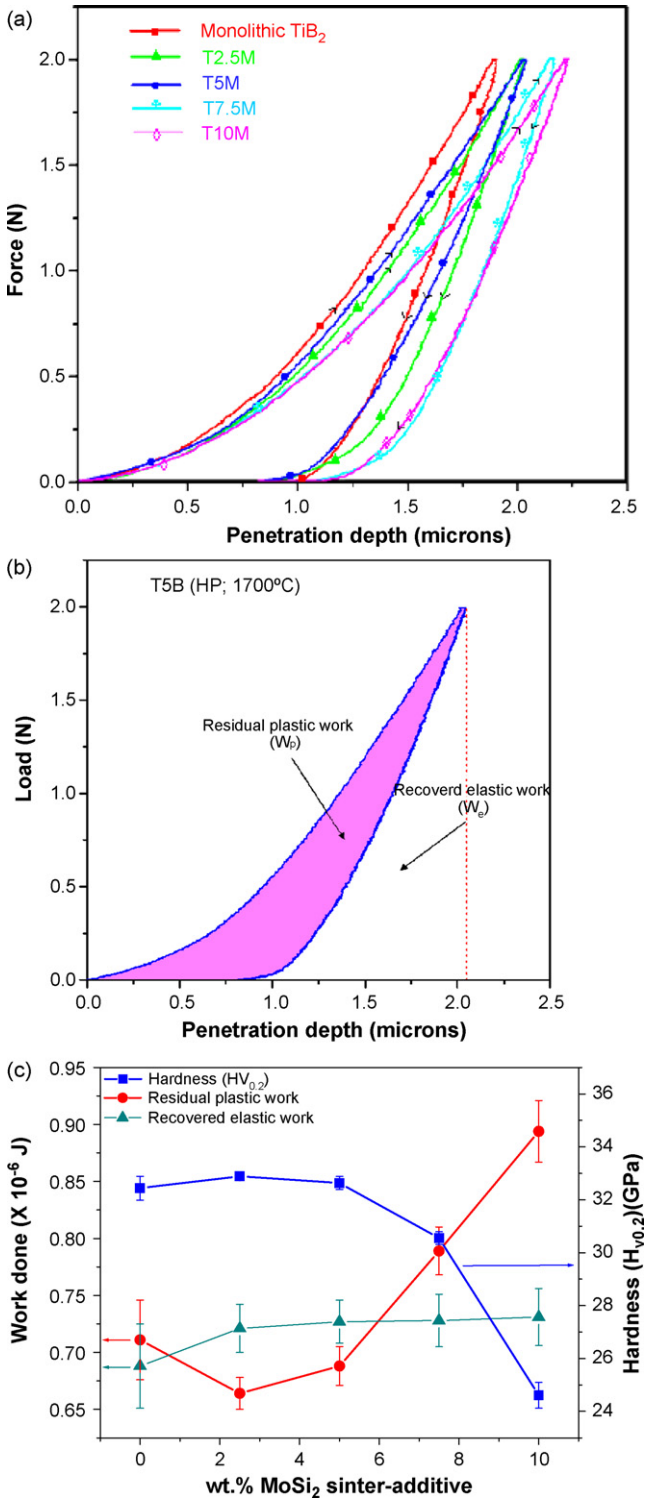

Fig. 5. (a) Load vs. penetration depth (P–d) plots, recorded for monolithic TiB_2 (HP; 1800 °C) and TiB_2-based composites (HP; 1700 °C) during instrumented Vickers indentation at a peak load of 2 N. (b) The areas corresponding to recoverable elastic work (W_e) and residual plastic work (W_p), performed during the instrumented indentation are indicated in a typical P–d plot. (c) The variation of the measured Vickers hardness ($H_{v0.2}$), W_e and W_p, with wt.% $MoSi_2$ (sinter-additive), as determined from the P–d curves of the densified (>95% ρ_{th}) TiB_2-based ceramics is presented.

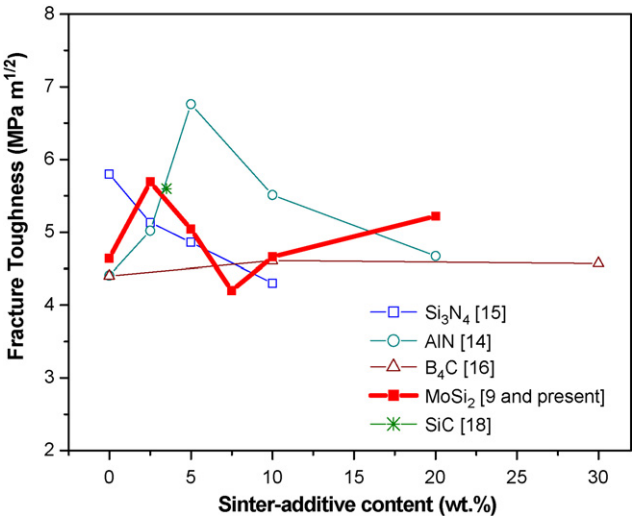

Fig. 6. Comparison between the fracture toughness achieved on using varying amounts of $MoSi_2$ and other ceramic additives as reinforcements for TiB_2.

4.2. Residual strain

Another possible effect of the presence of the secondary phases arises from the appreciable coefficient of thermal expansion mismatch ($\Delta\alpha$) between Mo_5Si_3 ($\alpha \sim 5 \times 10^{-6}\,K^{-1}$)[35] or Ti_5Si_3 ($\alpha \sim 22 \times 10^{-6}\,K^{-1}$)[36] and TiB_2 ($\alpha \sim 10 \times 10^{-6}\,K^{-1}$),[5] which results in the development of considerable elastic strain energy at the TiB_2/Ti_5Si_3 and TiB_2/Mo_5Si_3 interfaces during cooling from the fabrication temperature. Such residual strain developed at the grain boundaries might in turn lead to spontaneous grain boundary microcracking, if the strain exceeds some critical value (ε_{gbc}).[37]

The differential strain (ε_{gb}) set up near a grain boundary, due to coefficient of thermal expansion mismatch between the grains (phases) on either side of the boundary, is given by the following

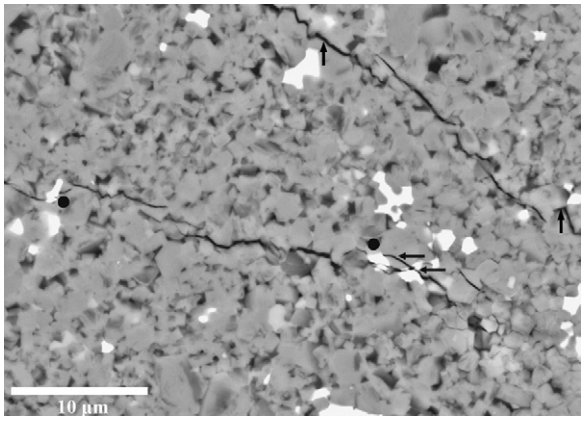

Fig. 7. Back scattered SEM image, corresponding to the polished surface of T10M, showing the influence of $MoSi_2$ sinter-additive on the propagation of a Vickers indentation (at 100 N) generated crack. Evidences of changes in crack path from intergranular to transgranular in the vicinity of $MoSi_2/Mo_5Si_3$ (brighter contrast) are indicated by arrows. Furthermore, crack bridging by $MoSi_2/Mo_5Si_3$ reinforcements is clearly observed and such evidences are indicated by dots.

expression[37]:

$$\varepsilon_{gb} = \frac{\Delta\alpha\,\Delta T}{(1-\nu)} \quad (2)$$

where ΔT is the temperature range over which the strain develops and ν is the Poisson's ratio (~0.2). In the present case, assuming that negligible plastic relaxation occurs for these ultrahard materials, ΔT corresponds to the difference between the hot pressing temperature and the final room temperature, and is approximately equal to 1650 °C. Now, considering that $\Delta\alpha$ between TiB_2 and Ti_5Si_3 is $\sim 12 \times 10^{-6}\,K^{-1}$ and that between TiB_2 and Mo_5Si_3 is $\sim 5 \times 10^{-6}\,K^{-1}$, the elastic strains developed at the respective interfaces are $\sim 24.9 \times 10^{-3}$ and $\sim 10.4 \times 10^{-3}$. On the other hand, the $\Delta\alpha$ between TiB_2 and $MoSi_2$ is $\sim 2 \times 10^{-6}\,K^{-1}$; which results in the development of a comparatively lesser strain of $\sim 4.2 \times 10^{-3}$ at the $TiB_2/MoSi_2$ interface.

Following the model proposed by Clarke,[38] the critical elastic strain (ε_{gbc}), set up near a grain boundary, resulting in spontaneous fracture along the boundary is given by

$$\varepsilon_{gbc} = \left(\frac{24\gamma_{gb}}{El_b}\right)^{1/2} \quad (3)$$

where, γ_{gb} is the grain boundary fracture energy, E is the elastic modulus and l_b is the length of the common interface between the two phases.

On close observation of the various micrographs showing the phase assemblage in the TiB_2-based composites, the average length of the common interface between the grey (TiB_2) phase and the brighter (Ti_5Si_3/Mo_5Si_3 or $MoSi_2$) phases (l_b) is found to be nearly ~1 μm. Assuming γ_{gb} as ~1 J/m^2, ε_{gbc} for the TiB_2-based composites can be roughly estimated to be $\sim 7.2 \times 10^{-3}$, which is lower than the elastic strains possibly developed at the TiB_2/Ti_5Si_3 and TiB_2/Mo_5Si_3 interface. Hence, the above calculations reveal that, although the $TiB_2/MoSi_2$ interfaces seem to be resistant from cracking, relatively larger residual strains along the TiB_2/Ti_5Si_3 and TiB_2/Mo_5Si_3 interfaces can lead to microcracking, especially at the indentation stress field.

As observed from the micrograph (Fig. 1c), due to the presence of higher volume fraction of TiB_2/Ti_5Si_3 and TiB_2/Mo_5Si_3 interfaces, such interfacial cracks are bound to have a considerable influence on the mechanical behaviour of the TiB_2-based composites developed from starting powders containing higher amount of $MoSi_2$. Accrued presence of such intergranular cracks should partially account for the deterioration of the fracture properties in the higher $MoSi_2$ containing ceramics. In fact, the observation of the additional contribution of intergranular fracture mode to the fracture of T10M, as compared to that of T5M, is in support of this argument (see Fig. 2). Hence, although $MoSi_2$ itself does not seem to result in degradation of the fracture properties of TiB_2-based composites, presence of considerable volume fraction of the reaction product phases deteriorates the fracture properties of TiB_2 above an optimum $MoSi_2$ sinter-additive content.

4.3. Work of indentation

From Table 2, it can be observed that with increase in $MoSi_2$ sinter-additive content, the total work done (W_t; estimated from the load vs. penetration (P–d) curves) during indentation increases. This is expected in light of the combination of lower stiffness and hardness of the secondary phases ($MoSi_2$, Mo_5Si_3 and Ti_5Si_3), which aids increased elastic as well as plastic deformation, respectively. However, Table 2 and Fig. 5c reveal that the amount of permanent plastic work (W_p; manifested in the form of permanent plastic depth remaining after complete removal of the load) is lower for the T2.5M and T5M composites with respect to that of monolithic TiB_2. Such observations are in accordance with the improvement in densification and hardness on reinforcement with small amount (2.5 and 5 wt.%) of $MoSi_2$. On the contrary, due to lower densification and presence of comparatively more amount of softer secondary phases, significantly larger amount of plastic work done can be performed during indentation of the higher $MoSi_2$ (>5 wt.%) reinforced composites. Another plausible reason for the accrued permanent deformation in these (higher $MoSi_2$ containing) composites lies in the presence of larger fraction of the brittle reaction product phases (Ti_5Si_3 and Mo_5Si_3), which might have resulted in the release of considerable amount of elastic strain energy via brittle fracture (microcracking) in the deformation zone. This suppresses the elastic recovery on release of the indentation load, which further contributes towards the significant increase in the measured residual plastic work, and hence reduction in hardness (H_v), for such materials.

With regard to the recovered elastic work done during indentation (W_e), it is observed that with addition of 2.5 wt.% $MoSi_2$, the elastic deformability increases quite sharply (as envisaged from the increased elastic recovery; Fig. 5c). However, with further increase in $MoSi_2$ sinter-additive content, a modest increment in W_e is noticed and most part of the work done during indentation remains as residual plastic work. Comparison of this observation with the variation of elastic modulus, with $MoSi_2$ content (Table 2), does not totally agree with the normally expected inverse relationship between recoverable elastic deformation and E. We believe that this discrepancy once again lies in the presence of considerably higher volume fraction of the secondary phases in such composites. Possible fracturing in the deformation zone might result in increased unrecoverable (plastic) macro-deformation. In other words, although the initial elastic deformation might have been more pronounced for such composites, the enhanced release of the elastic strain energy via brittle fracture restricted the recovery to some extent upon unloading. Hence, the measured elastic recovery might not exactly account for the elastic deformability of these higher $MoSi_2$ containing composites.

4.4. Indentation-size effect

The experimentally measured Vickers hardness values, estimated using indentations performed at varying indent loads (2–100 N), have revealed considerable variation with indentation load for all the materials (see Table 1 and Fig. 4). It has been

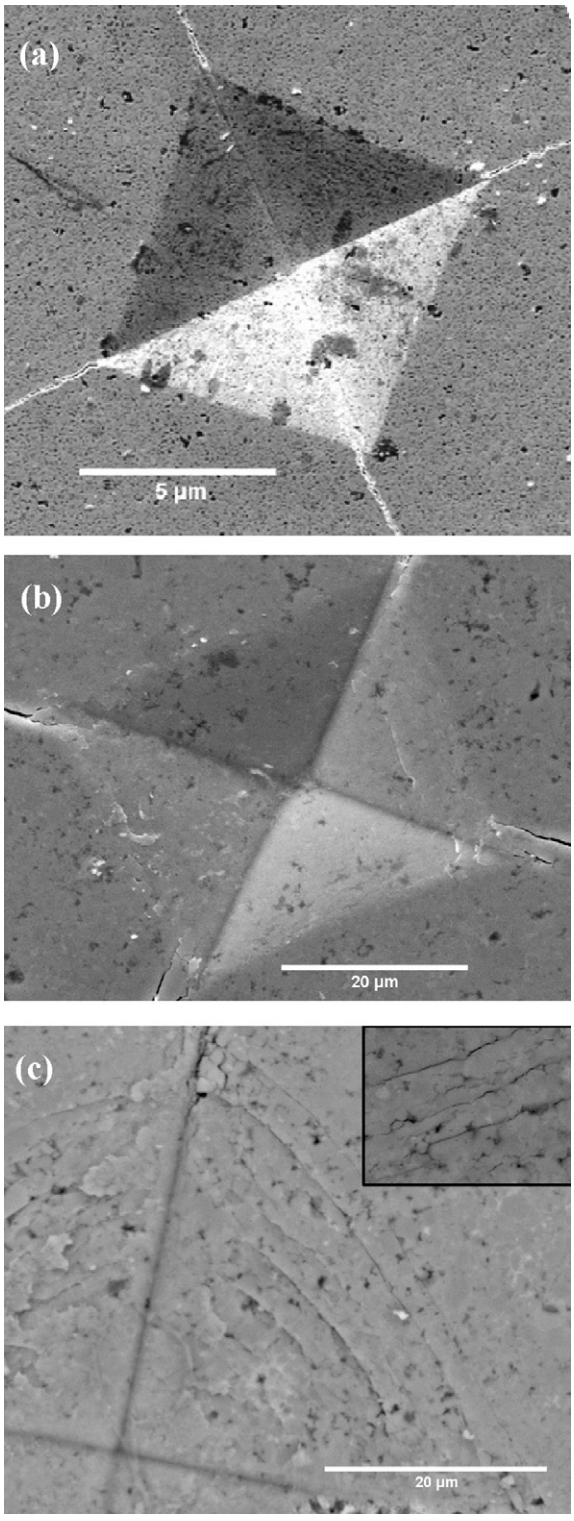

Fig. 8. Typical Vickers indents obtained on T2.5M (HP; 1700 °C) at indent loads of (a) 2 N, (b) 50 N, (c) 100 N. Note the presence of concentric array of cracks, running parallel to each other, within the indent (at the indent faces) obtained at 100 N.

observed that hardness decreases with increasing indent load and therefore, all the densified materials exhibit 'indentation size effect'. Such size/load effects of Vickers hardness for different ceramic materials have also been reported earlier,[39–41] whereby such observations have been attributed to the occurrence of the easier process of multiplication of sufficient number of pre-existing elements of plasticity (dislocations, twins) at higher loads, in contrast to the more difficult process of generating new dislocations in the vicinity of indents at lower loads. Though we do not completely preclude the possibility of such occurrences leading to the indentation 'load/size effect' observed in our materials, here we propose another mechanism which should definitely account for the present observations, especially in light of the fact that the materials under consideration are hard and brittle covalently bonded ceramics.

Careful observation of the Vickers indentations, obtained at the various loads (see Fig. 8), reveal that indentations obtained with T2.5M, at the lower indent loads of 2 and 50 N are nearly 'perfect' (Fig. 8a and b). Other than the radial cracks emanating from the corner of such indents, no additional cracking can be observed in the vicinity of the 'plastically' deformed region. However, in addition to such radial cracking, presence of a concentric array of cracks, running parallel to each other, can be observed within the indents (at the faces) obtained at an indent load of 100 N (Fig. 8c). The above observations point towards the increased severity of surface and subsurface cracking, in the vicinity of indents, with increase in indent load. It must be noted that in addition to suppressing elastic recovery due to release of strain energy, such considerable crack openings (at the indent faces) result in additional displacements, which is manifested at the macro level as permanent (plastic) deformation. These observations further support and supplement the arguments developed above that such enhanced cracking, occurring during indentation cycle and remaining after removal of indentation load, contribute to the additional permanent (residual) deformation measured at the higher indent load. It must also be mentioned here that Ritcher et al.[41] recorded a similar observation of intergranular cracking within Vickers indents, obtained at higher loads on transition metal carbides. Such cracking was believed to contribute towards the measured permanent deformation and hence the estimated comparatively lower hardness values. Hence, correlation of the hardness behaviour with critical observation of the Vickers indents of the respective materials obtained at different indent loads, provide evidences in support of the view that occurrence of microcracking in the vicinity of indents influences the residual macro-deformation and concomitantly the measured hardness of these hard and brittle materials.

5. Conclusions

The present research, devoted towards the in-detail study of the effects of sinter densities, composition ($MoSi_2$ sinter-additive content), phase assemblage and microstructural development on the mechanical behaviour of TiB_2-based ceramics/composites, has lead to the following major conclusions.

The incorporation of 2.5 wt.% $MoSi_2$, as sinter-additive, in TiB_2 leads to near theoretical densification and notable

improvements in the mechanical properties with respect to monolithic TiB_2. However, the degradation in mechanical properties with increase in $MoSi_2$ content, beyond 5 wt.%, is critically recorded.

The optimized TiB_2–2.5 wt.% $MoSi_2$ exhibits good combination of mechanical properties such as high hardness ($H_{v5} \sim 29$ GPa) and elastic modulus ($E \sim 490$ GPa), along with considerably improved fracture properties in terms of fracture toughness (~ 6 MPa $m^{1/2}$) and flexural strength (~ 400 MPa).

Critical analysis reveals that the degradation of mechanical properties correlate well with the presence of higher volume fraction of porosities (lower sinter densities) and brittle reaction product phases (Ti_5Si_3 and Mo_5Si_3). The presence of Ti_5Si_3 and Mo_5Si_3, having considerably different coefficient of thermal expansion with respect to TiB_2, results in the development of significant residual strain at the corresponding interfaces. Such residual strains are quite likely to lead spontaneous microcracking along such interfaces and hence play a role in degrading the mechanical behaviour of the TiB_2-based composites, reinforced with higher volume fraction of $MoSi_2$ (sinter-additive).

An important observation has been the considerably lower Vickers hardness, measured with indents obtained at higher loads (100 N), as compared to those measured with indents obtained at lower loads (2 and 50 N) for all the densified materials. The extent of 'indentation load/size' effect is found to depend on the relative amounts of the various microstructural constituents ($MoSi_2$, secondary phases and porosity). The possible contribution of concentric cracking, as observed in the vicinity of the indents (faces) obtained at the higher loads, to such 'indentation load/size effects' has been demonstrated.

Acknowledgements

The financial support by Board of Research in Nuclear Science (BRNS) programme of Department of Atomic Energy (DAE), Government of India is gratefully acknowledged. The authors wish to thank Prof. U. Ramamurthy, Materials Engineering, Indian Institute of Science for allowing us to use instrumented hardness testing machine.

References

1. Cutler, R. A., Engineering properties of borides. In *Engineered Materials Handbook*. Vol. 4. *Ceramics and Glasses*. ASM International. The Materials Information Society, USA; 1991.
2. Basu, B., Raju, G. B. and Suri, A. K., Processing and properties of monolithic TiB_2-based materials. *Int. Mater. Rev.*, 2006, **51**, 352–374.
3. Munro, R. G., Material properties of titanium diboride. *J. Res. Nat. Inst. Stand. Tech.*, 2000, **105**(5), 709–720.
4. Murthy, T. S. R. Ch., Balasubramaniam, R., Basu, B., Suri, A. K. and Mungole, M. N., Oxidation of monolithic TiB_2 and TiB_2–20 wt.% $MoSi_2$ composite at 850 °C. *J. Eur. Ceram. Soc.*, 2006, **26**(1–2), 187–192.
5. Feber, M. K., Becher, P. F. and Finch, C. B., Effect of microstructure on the properties of TiB_2 ceramics. *J. Am. Ceram. Soc.*, 1983, **66**(1), C2–C4.
6. Telle, R., Boride and carbide ceramics. In *Materials Science and Technology*. Vol. 11. *Structure and Properties of Ceramics*, ed. R. W. Cahn, P. Haasen, and E. J. Kramer. Swain VCH, Weinheim, Germany, 1994, p. 175.
7. Baik, S. and Becher, P. F., Effect of oxygen contamination on densification of TiB_2. *J. Am. Ceram. Soc.*, 1987, **70**(8), 527–530.
8. Wang, W., Fu, Z., Wang, H. and Yuan, R., Influence of hot pressing sintering temperature and time on microstructure and mechanical properties of TiB_2 ceramics. *J. Eur. Ceram. Soc.*, 2002, **22**, 1045–1049.
9. Murthy, T. S. R. Ch., Basu, B., Balasubramaniam, R., Suri, A. K., Subramanian, C. and Fotedar, R. K., Processing and properties of TiB_2 with $MoSi_2$ sinter-additive: a first report. *J. Am. Ceram. Soc.*, 2006, **89**(1), 131–138.
10. Petzow, G., Telle, R., New development in the field of refractory hard metals based on cemented borides. In *Advanced Ceramics*, ed. S. Somiya. Tokyo, 1987, p. 131–43.
11. Einarsrud, M., Hagen, E., Petterson, G. and Grande, T., Pressureless sintering of titanium diboride with nickel, nickel boride, and iron additives. *J. Am. Ceram. Soc.*, 1997, **80**(12), 3013–3020.
12. Kang, S. H., Kim, D. J., Kang, E. S. and Baek, S. S., Pressureless sintering and properties of titanium diboride ceramics containing chromium and iron. *J. Am. Ceram. Soc.*, 2001, **84**(4), 893–895.
13. Baumgartner, H. R. and Steiger, R. A., Sintering and properties of titanium diboride made from powder synthesized in a plasma-arc heater. *J. Am. Ceram. Soc.*, 1984, **67**(3), 207–212.
14. Li, L. H., Kim, H. E. and Kang, E. S., Sintering and mechanical properties of titanium diboride with aluminum nitride as a sintering aid. *J. Eur. Ceram. Soc.*, 2002, **22**, 973–977.
15. Park, J. H., Koh, Y. H., Kim, H. E., Hwang, C. S. and Kong, E., Densification and mechanical properties of titanium diboride with silicon nitride as a sintering aid. *J. Am. Ceram. Soc.*, 1999, **82**(11), 3037–3042.
16. Tuffe, S., Dubois, J., Fantozzi, G. and Barbier, G., Densification, microstructure and mechanical properties of TiB_2–B_4C based composites. *Int. J. Ref. Met. Hard. Mater.*, 1996, **14**, 305–310.
17. Kim, H. J., Choi, H. J. and Lee, J. G., Mechanochemical synthesis and pressureless sintering of TiB_2–AlN composites. *J. Am. Ceram. Soc.*, 2002, **85**(4), 1022–1024.
18. Basu, B., Vleugels, J. and Vanderbiest, O., Fretting wear behaviour of TiB_2-based materials against bearing steel under water and oil lubrication. *Wear*, 2001, **250**, 631–641.
19. Murata, Y., Julien, H. P. and Whitney, E. D., Densification and wear resistance of ceramic systems. I. Titanium diboride. *Ceram. Bull.*, 1967, **46**(7), 643–648s.
20. Mitra, R., Prasad, N. E., Kumari, S. and Rao, A. V., High-temperature deformation behaviour of coarse and fine-grained $MoSi_2$ with different silica contents. *Metal. Mater. Trans. A*, 2003, **34**, 1069–1088.
21. Anstis, G. R., Chantukul, P., Lawn, B. R. and Marshall, D. B., A critical evaluation of indentation techniques for measuring fracture toughness. I. Direct crack measurements. *J. Am. Ceram. Soc.*, 1981, **64**, 533–538.
22. Evans, A. G. and Charles, E. A., Fracture toughness determinations by indentation. *J. Am. Ceram. Soc.*, 1976, **59**(7–8), 371–372.
23. Niihara, K., Morena, R. and Hasselman, D. P. H., Evaluation of K_{Ic} of brittle solids by the indentation method with low crack-to-indent ratios. *J. Mater. Sci. Lett.*, 1982, **1**, 13–16.
24. Jones, S. L., Norman, C. J. and Shahani, R., Crack-profile shapes formed under a Vickers indent pyramid. *J. Mater. Sci. Lett.*, 1987, **6**, 721–723.
25. Mukhopadhyay, A., Basu, B., Bakshi, S. D. and Mishra, S. K., *Int. J. Ref. Met. Hard. Mater.*, 2007, **25**, 179–188.
26. Telle, R., Meyer, S., Petzow, G. and Fran, E. D., Sintering behaviour and phase reactions of TiB_2 with ZrO_2 additives. *Mater. Sci. Eng. A*, 1998, **105/106**, 125–129.
27. Konigshofer, R., Furnsinn, S., Steinkellner, P., Lengauer, W., Haas, R., Rabitsch, K. and Scheerer, M., Solid-state properties of hot-pressed TiB_2 ceramics. *Int. J. Ref. Met. Hard. Mater.*, 2005, **23**, 350–357.
28. Riedel, R., *Handbook of Ceramic Hard Materials*. Vol. 2. Wiley–VCH Verlag GmbH, Weinheim (Federal Republic of Germany), 2000, p. 968–90.
29. Chollacoop, N., Dao, M. and Suresh, S., Depth-sensing instrumented indentation with dual sharp indenters. *Acta Mater.*, 2003, **51**, 3713–3729.
30. Oliver, W. C. and Pharr, G. M., An improved technique for determining hardness and elastic modulus using load and displacement sensing indentation experiments. *J. Mater. Res.*, 1992, **7**(6), 1564–1583.
31. Pharr, G. M., Oliver, W. C. and Brotzen, F. R., On the generality of the relationship among contact stiffness, contact area, and elastic modulus during indentation. *J. Mater. Res.*, 1992, **7**(3), 613–617.

32. Oliver, W. C. and Pharr, G. M., Measurement of hardness and elastic modulus by instrumented indentation: advances in understanding and refinements in methodology. *J. Mater. Res.*, 2004, **19**(1), 3–20.
33. Venkatesh, T. A., Vliet, K. J. V., Giannakopoulos, A. E. and Suresh, S., Determination of elasto-plastic properties by instrumented sharp indentation: guidelines for property extraction. *Scripta Mater.*, 2000, **42**, 833–839.
34. Zeng, K. and Chiu, C. H., An analysis of load–penetration curves from instrumented indentation. *Acta Mater.*, 2001, **49**, 3539–3551.
35. Iizuka, T., Murao, T., Yamamoto, H. and Kita, H., Microstructures and properties of Mo_5Si_3-particle reinforced Si_3N_4-matrix composites. *J. Am. Ceram. Soc.*, 2002, **85**(4), 954–960.
36. Raju, G. B. and Basu, B., Densification, sintering reactions and properties of titanium diboride with titanium disilicide as a sintering aid. *J. Am. Ceram. Soc.*, 2007, **90**(11), 3415–3423.
37. Davidge, R. W., Mechanical behaviour of ceramics. In *Cambridge Solid State Science Series*, ed. R. W. Cahn, M. W. Thompson and I. M. Ward. University Press, Cambridge, 1979.
38. Clarke, F. J. P., Residual strain and the fracture stress-grain size relationship in brittle solids. *Acta Metall.*, 1964, **12**, 139–143.
39. Krell, A., A new look at grain size and load effects in the hardness of ceramics. *Mater. Sci. Eng. A*, 1998, **245**, 277–284.
40. Carpinetri, A. and Puzzi, S., A fractal approach to indentation size effect. *Eng. Fract. Mech.*, 2006, **73**(15), 2110–2122.
41. Ritcher, V. and Ruthendorf, M. V., On hardness and toughness of ultrafine and nanocrystalline hard materials. *Int. J. Ref. Met. Hard. Mater.*, 1999, **17**, 141–152.